

## Real-Space and Reciprocal-Space Berry Phases in the Hall Effect of $\text{Mn}_{1-x}\text{Fe}_x\text{Si}$

C. Franz,<sup>1</sup> F. Freimuth,<sup>2</sup> A. Bauer,<sup>1</sup> R. Ritz,<sup>1</sup> C. Schnarr,<sup>1</sup> C. Duvinage,<sup>1</sup> T. Adams,<sup>1</sup> S. Blügel,<sup>2</sup>  
A. Rosch,<sup>3</sup> Y. Mokrousov,<sup>2</sup> and C. Pfleiderer<sup>1</sup>

<sup>1</sup>*Physik-Department, Technische Universität München, James-Frank-Strasse, D-85748 Garching, Germany*

<sup>2</sup>*Institute for Advanced Simulation and Peter Grünberg Institut,  
Forschungszentrum Jülich and JARA, D-52425 Jülich, Germany*

<sup>3</sup>*Institute for Theoretical Physics, Universität zu Köln, Zülpicher Strasse 77, D-50937 Köln, Germany*

(Received 9 December 2013; published 8 May 2014)

We report an experimental and computational study of the Hall effect in  $\text{Mn}_{1-x}\text{Fe}_x\text{Si}$ , as complemented by measurements in  $\text{Mn}_{1-x}\text{Co}_x\text{Si}$ , when helimagnetic order is suppressed under substitutional doping. For small  $x$  the anomalous Hall effect (AHE) and the topological Hall effect (THE) change sign. Under larger doping the AHE remains small and consistent with the magnetization, while the THE grows by over a factor of 10. Both the sign and the magnitude of the AHE and the THE are in excellent agreement with calculations based on density functional theory. Our study provides the long-sought material-specific microscopic justification that, while the AHE is due to the reciprocal-space Berry curvature, the THE originates in real-space Berry phases.

DOI: 10.1103/PhysRevLett.112.186601

PACS numbers: 72.15.-v, 71.15.Mb, 71.20.Be

Measurements of the Hall effect in chiral magnets with B20 crystal structure have recently attracted great interest [1–7]. Because of a hierarchy of energy scales [8], comprising in decreasing strength ferromagnetic exchange, Dzyaloshinsky-Moriya spin-orbit interactions, and higher order spin-orbit coupling terms, magnetic order in these systems displays generically long-wavelength helical modulations. Under a small applied magnetic field this hierarchy of energy scales stabilizes a Skyrmion lattice phase (SLP) in the vicinity of the magnetic transition temperature, i.e., a lattice composed of topologically nontrivial whirls of the magnetization [9–16]. The Hall effect, which has been studied most extensively in MnSi [1–3,17–19], displays thereby three contributions, notably an ordinary Hall effect (OHE), an anomalous Hall effect (AHE) related to the uniform magnetization, and an additional topological Hall effect (THE) in the SLP due to the nontrivial topology of the spin order.

It was only recently noticed that the THE and AHE represent the real- and reciprocal-space limits of generalized phase-space Berry phases of the conduction electrons, respectively. First principles calculations in MnSi suggest that these phase-space Berry phases account quantitatively for the Dzyaloshinsky-Moriya interaction and may even give rise to an electric charge of the Skyrmions [20,21]. However, so far perhaps most spectacular because of the experimental evidence is the notion that the nontrivial topological winding of Skyrmions gives rise to Berry phases in real space that may be viewed as an emergent magnetic field  $B^{\text{eff}} = \Phi_0 \Phi$  of one flux quantum ( $\Phi_0 = h/e$ ) times the winding number  $\Phi = -1$  per Skyrmion [1]. The same mechanism also leads to large spin transfer torques in MnSi [22,23] and FeGe at ultralow current densities. In turn, a very large THE in

MnGe [4] and SrFeO<sub>3</sub> [5] has fueled speculations that the emergent fields may even approach the quantum limit.

Despite this wide range of interest, the account of Berry phases in the Hall effect has been essentially phenomenological, in particular for the THE, while a material-specific microscopic justification has been missing. This situation is aggravated by the microscopic sensitivity of the THE to at least three factors: (i) details of the Fermi surface topology, (ii) differences of the average charge carrier lifetime on each Fermi surface sheet, and (iii) a breakdown of the adiabatic approximation due to spin-flip scattering and possible mixtures of real- and reciprocal-space Berry phases when spin-orbit coupling becomes comparable to the exchange splitting [2].

In this Letter, we report a combined experimental and theoretical study of the Hall effect in  $\text{Mn}_{1-x}\text{Fe}_x\text{Si}$ , supported by complementary Hall data in  $\text{Mn}_{1-x}\text{Co}_x\text{Si}$ . As our main results we find for small  $x$  a change of sign of both the AHE and THE, however, at slightly different compositions. For larger  $x$  we find that the AHE is small consistent with the magnetization, while the magnitude of the THE grows and exceeds that of pure MnSi by over a factor of 10. Using density functional theory we are able to account for both the magnitude as well as the sign of the THE and AHE observed experimentally. The doping dependence can thereby be related to changes in the ordinary Hall conductivity and a redistribution of  $d$  states at the Fermi energy as discussed below. Taken together our study provides the long-sought microscopic justification for the phenomenological description of the THE and AHE as the real- and reciprocal-space limits of general phase-space Berry phases, with the additional surprise that this occurs in the same complex material.

For a summary of the experimental methods, which follow the procedures reported in Refs. [2,3,24–26], we refer to the Supplemental Material [27]. Shown in Fig. 1 is an overview of typical magnetization, and Hall resistivity data as well as magnetic phase diagrams (a detailed list of the temperature values and parameters studied is part of the Supplemental Material [27]). The evolution of the magnetization  $m$  at selected temperatures and selected Fe and Co concentrations is shown in panels (a1) through (a5). At the lowest temperatures  $m$  changes from an almost linear increase to being almost field independent when going from below to above  $B_{c2}$ . With increasing  $x$  the magnetization at the lowest temperatures decreases, characteristic of a decrease of the ordered moment [see also Fig. 2(f) below]. The susceptibility calculated from  $m$  compares well with the ac susceptibility (both not shown), thus permitting us to deduce the magnetic phase diagrams as depicted in Fig. 1, panels (b1) through (b5) (cf. Ref. [24]). Here the usual magnetic phases are distinguished following accurately previous work [24–26], notably paramagnetism (PM), helimagnetic order ( $h$ ), Skyrmion lattice phase (SLP), conical order, field-induced ferromagnetism (FM), and the fluctuation-disorder crossover regime (FD) [28].

The Hall resistivity  $\rho_{xy}$ , shown in Fig. 1, panels (c1) through (c5), displays considerable variations. To permit

direct comparison of  $m$  with  $\rho_{xy}$  all data have been corrected for the effects of demagnetizing fields. We begin at high temperatures, where  $\rho_{xy}$  is essentially linear and dominated by the OHE without much change as a function of  $x$ . With decreasing temperature an additional contribution emerges in striking similarity with  $m$ , the AHE. As a key observation the sign of the AHE changes from positive to negative between  $x = 0.04$  and  $0.06$  under Fe doping (in Fig. 1 it qualitatively resembles the mirror image of  $m$  for  $x \geq 0.08$ ; this AHE changes sign between  $x = 0.02$  and  $0.04$  under Co doping). Finally, a third contribution in  $\rho_{xy}$  on top of the OHE and AHE may be distinguished, which for pure MnSi and low concentrations is strictly confined to the SLP. The relevant phase boundaries of the SLP inferred from the susceptibility are marked by vertical lines in Fig. 1. For all Fe concentrations  $x \geq 0.04$  (under Co doping  $x \geq 0.02$ ) this THE is negative (downwards) with increasing magnitude [cf. Fig. 1, panels (c2) to (c5)] consistent with previous work [27]. In contrast, for the pure compound the THE is positive (upwards) as shown in great detail in Refs. [1–3], where the THE for  $x = 0$  cannot be resolved on the scale of Fig. 1 (c1). Hence, the THE changes sign as a function of  $x$ , however, at a smaller composition than the AHE.

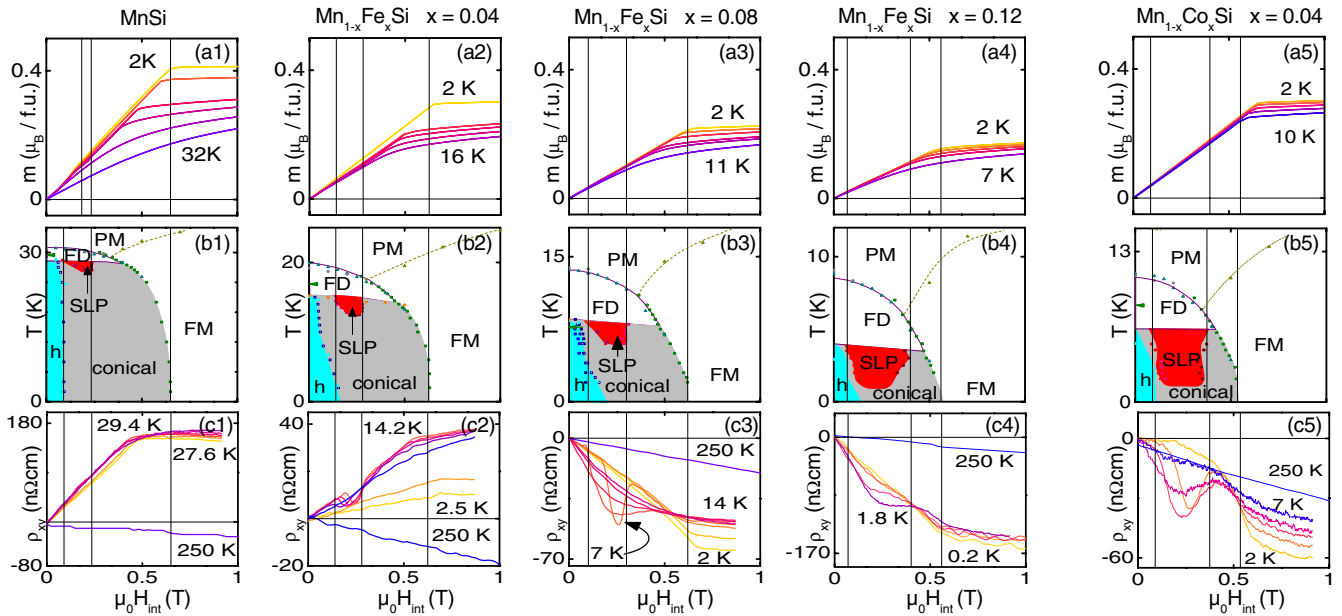


FIG. 1 (color online). Doping dependence of  $m$ , the magnetic phase diagram, and  $\rho_{xy}$  of  $\text{Mn}_{1-x}\text{Fe}_x\text{Si}$  and  $\text{Mn}_{1-x}\text{Co}_x\text{Si}$  at selected  $x$ . Panels (a1) through (a5): Magnetization at selected temperatures in the vicinity of the helimagnetic transition. Panels (b1) through (b5): Magnetic phase diagrams as inferred from the susceptibility calculated numerically from the magnetization (see also Ref. [24]). Panels (c1) through (c5): Typical Hall resistivity at selected temperatures (see [27] for detailed list of temperatures). At low temperatures the Hall resistivity is dominated by the AHE, which tracks qualitatively the magnetization. Between  $x = 0.04$  and  $0.08$  the sign of this AHE changes from positive to negative; i.e., it assumes qualitatively the shape of a mirror image of  $m$ . In the field range of the Skyrmion lattice phase (SLP), marked by vertical lines, a THE exists in the form of an additional contribution directed downwards for all  $x \geq 0.04$ . For  $x = 0$  the THE points upwards (cf. Fig. 2 in Ref. [1]), which cannot be resolved on the scale used here; i.e., the THE also changes sign as a function of  $x$ .

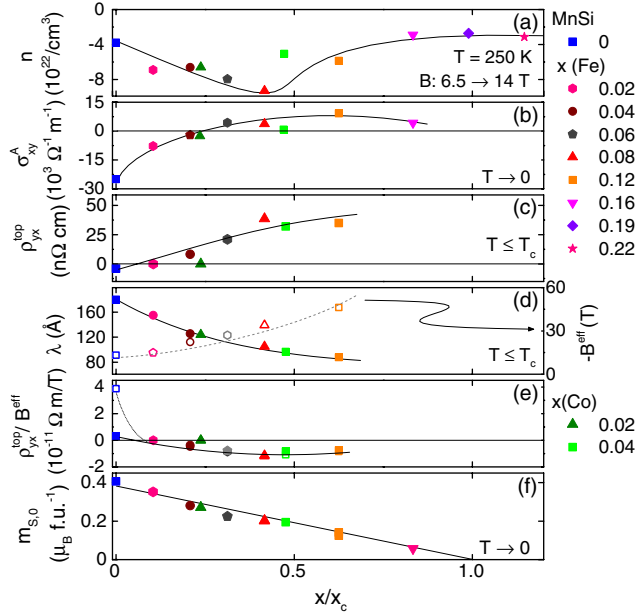


FIG. 2 (color online). Main features characterizing the variation of the Hall effects in  $\text{Mn}_{1-x}\text{Fe}_x\text{Si}$  and  $\text{Mn}_{1-x}\text{Co}_x\text{Si}$  as a function of normalized composition  $x/x_c$ . See text for details.

As the scope of our Letter is the microscopic underpinning of the AHE and THE, we do not address the properties for  $x \rightarrow x_c$ , where  $T_c$  is suppressed to zero. Nonetheless, it is interesting to note that the THE is already present in the fluctuation disordered (FD) regime under Fe doping, e.g., up to  $\sim 10$  K for  $x = 0.08$  where  $T_c = 8.8$  K (cf. table of temperature values in the Supplemental Material [27]). This behavior is reminiscent of recent high pressure studies in MnSi, where a THE emerges at high pressure above  $T_c$  [3]. Further, in the FD regime the THE extends over a much larger field range as compared to the SLP; for  $x = 0.12$  it clearly emerges around  $B = 0$  at temperatures down to  $T \approx 0.6$  K, below which it vanishes.

Summarized in Fig. 2 are the salient features of all of our experimental data on the OHE, AHE, and THE. We begin by considering charge carrier concentration  $n$  inferred from  $\rho_{xy}$  at 250 K in the range 6 and 14 T, i.e., far from the temperature and field range of interest and where it is dominated by the OHE. As shown in Fig. 2(a)  $n$  displays only a gradual reduction by a factor of 2 around  $x/x_c \approx 0.5$ . This suggests strongly that the electronic structure does not change radically under doping. Unfortunately, it is not possible to obtain any additional information on the OHE at low temperatures and fields, since the AHE and THE are large.

To capture the AHE we consider the Hall conductivity  $\sigma_{xy} = \rho_{yx}/(\rho_{xx}^2 + \rho_{xy}^2)$  and determine the anomalous contribution  $\sigma_{xy}^A$  by extrapolating  $\sigma_{xy}$  from  $B > B_{c2}$  to zero field; i.e., we extrapolate from the field-polarized state to zero field.  $\sigma_{xy}^A$  obtained this way increases from a large negative value at  $x = 0$ , changes sign between  $x = 0.04$

and 0.06, and approaches a small positive value for large  $x$  as shown in Fig. 2(b). We note that the AHE is large in  $\rho_{xy}$  even for low temperatures [cf. Fig. 1, panels (c2) through (c5)], because the residual resistivity increases under doping and approaches  $\sim 80 \mu\Omega \text{ cm}$  near  $x_c$  [29]. Third, we determined the size of the THE,  $\rho_{yx}^{\text{top}}$ , in the center of the SLP as described in Refs. [2] and [3]. With increasing doping  $\rho_{yx}^{\text{top}}$  changes sign between  $x = 0$  and 0.02, i.e., at a different composition than the AHE. This is followed by an increase of  $\rho_{yx}^{\text{top}}$  by a factor of 10 when increasing  $x$  further [Fig. 2(c)] [30].

The large increase of  $\rho_{yx}^{\text{top}}$  is partly related to the reduction of the helical wavelength  $\lambda$  as determined by small-angle neutron scattering [Fig. 2(d)], where  $\lambda$  is found to decrease by a factor of 2 under doping. Data shown in Fig. 2(d) were measured at the instruments RESEDA and MIRA at FRM II, Munich [31,32]. Thus, the emergent magnetic field  $B^{\text{eff}} \sim 1/\lambda^2$  increases by a factor of 4 from  $-13$  to about  $-60$  T over the range of interest as the area per emergent flux quantum  $\Phi_0$  decreases. Shown in Fig. 2(e) is  $\rho_{yx}^{\text{top}}/B^{\text{eff}}$  including an estimate of the effects of finite temperature [27] since the temperature at which the SLP forms decreases with increasing  $x$ . The estimated zero-temperature values are shown by open symbols. However, the correction is only large for  $x = 0$ , where it was inferred from the pressure dependence [2,33], while it is not even noticeable in the doped samples. In turn, the discussion and conclusions presented below do not depend on finite temperature effects. As a final piece of information needed below we show in Fig. 2(f) the extrapolated ordered moment in the zero-temperature limit.

In view of the possible microscopic sensitivity of the THE described above [2] we have also considered the Hall effect under Co doping. In a previous study it was found that the temperature versus composition phase diagram, as well as the associated magnetic phase diagrams of  $\text{Mn}_{1-x}\text{Fe}_x\text{Si}$  and  $\text{Mn}_{1-x}\text{Co}_x\text{Si}$ , are remarkably similar [24]. Yet the critical concentration  $x_c$  needed to suppress the helimagnetic transition is a factor of 2 smaller under Co doping. Extending this analogy we find that the sign and magnitude of the AHE and THE as a function of reduced Co concentration,  $x/x_c$  also correspond to Fe doping as illustrated in Figs. 1(a5), 1(b5), and 1(c5) as well as in Fig. 2. This analogy suggests empirically that the detailed relaxation rates are not dominantly responsible for the evolution of the Hall effect under doping.

For the comparison with experiment we calculated the electronic structure of collinear ferromagnetic MnSi within the full-potential linearized augmented plane-wave method as implemented in the Jülich density functional (DFT) code FLEUR. The electronic structure of MnSi was computed within the local density approximation to DFT at the experimental lattice constant,  $a = 4.558 \text{ \AA}$ . Further, the effect of doping with Fe was taken into account within the virtual crystal approximation (VCA) of MnSi, in terms

of a fractional change of the nuclear number at the Mn site proportional to the Fe concentration. Thus, in VCA, adding Fe results in an effective tuning of the electronic structure and Fermi surface topology of pure MnSi, while the details of microscopic electron scattering off Fe impurities are not taken into account. Within VCA, the difference of Co and Fe doping of MnSi arises then from the different nuclear charge of the Mn atoms, and the electronic structure of  $\text{Mn}_{1-x}\text{Co}_x\text{Si}$  effectively corresponds to the electronic structure of  $\text{Mn}_{1-2x}\text{Fe}_{2x}\text{Si}$ . The approximations made in describing the doping of MnSi with Co and Fe are in turn strongly supported by our experimental results as discussed above.

For each concentration  $x$  we finally constrained the spin moment to the experimental values shown in Fig. 2(f) (see also [27]), where the unconstrained LDA overestimates the spin moments by more than a factor of 2. To compute the Hall conductivities an interpolation based on Wannier functions [34] was used. Further computational details are provided in [27].

To confirm that the LDA with constrained spin moment describes the electronic structure correctly, we computed at first the anomalous Hall conductivity (AHC) in ferromagnetic  $\text{Mn}_{1-x}\text{Fe}_x\text{Si}$ , providing a property that is extremely sensitive to the Fermi surface, and compared it with experiment as shown in Figs. 3(a) and 3(b). Namely, we computed the intrinsic contribution to the AHC by evaluating the Berry curvature of the occupied states, neglecting the skew-scattering contribution to the AHE. The latter is suppressed for ferromagnets away from the clean regime, as expected in doped systems like  $\text{Mn}_{1-x}\text{Fe}_x\text{Si}$ . We have further estimated the extrinsic side-jump contribution to the AHE and find not more than 10% of the intrinsic values [35]. Hence, the calculated AHC is in excellent agreement with experiment as concerns (i) the magnitude, (ii) the change of sign, and (iii) the reduction of the AHC under Fe doping.

We turn now to the topological Hall constant as determined by Boltzmann transport theory within the

constant relaxation time approximation. The latter relies on the assumption that for each spin the relaxation rates of all states at the Fermi surface are the same. Within this approximation the spin-resolved diagonal conductivity is then given by a product of the common relaxation time  $\tau_s$  [ $s = (\uparrow, \downarrow)$ ] and a term which is determined by the Fermi surface topology only:

$$\sigma_{xx}^s = \frac{e^2}{VN} \sum_{\mathbf{k}n} \tau_s \delta(E_F - \epsilon_{\mathbf{k}ns}) (v_{\mathbf{k}ns}^x)^2, \quad (1)$$

where  $V$  is the unit cell volume,  $N$  is the number of  $\mathbf{k}$  points in the Brillouin zone,  $E_F$  is the Fermi energy,  $\epsilon_{\mathbf{k}ns}$  is the band energy of band  $n$  at  $\mathbf{k}$ , and  $v_{\mathbf{k}ns}^x$  is the group velocity in  $x$  direction of this state. We assume that  $\tau_s = \alpha \eta_s^{-1}$ , where  $\eta_s$  is the density of states at  $E_F$  for spin  $s$  and  $\alpha$  is a constant. In turn, the ordinary Hall conductivity at a given magnetic field  $B^z$  may be expressed as

$$\sigma_{xy}^{\text{OHE},s}(B^z) = -\frac{e^3 B^z}{VN} \sum_{\mathbf{k}n} \tau_s^2 \delta(E_F - \epsilon_{\mathbf{k}ns}) \times [(v_{\mathbf{k}ns}^x)^2 m_{\mathbf{k}ns}^{yy} - v_{\mathbf{k}ns}^x v_{\mathbf{k}ns}^y m_{\mathbf{k}ns}^{xy}], \quad (2)$$

with the inverse effective mass tensor  $m_{\mathbf{k}ns}^{ij} = \partial^2 \epsilon_{\mathbf{k}ns} / (\hbar^2 \partial k_i \partial k_j)$ . The experimentally measured THE has been attributed phenomenologically to the Lorentz force caused by the emergent magnetic field  $\mathbf{B}^{\text{eff}} = B^{\text{eff},z}$  associated with the spin texture. This force is opposite for electrons of opposite spin due to the topological charge of the Skyrmion, which governs the problem in the space of the magnetization direction. The topological Hall resistivity as approximated by the difference of the OHE for spin-up and spin-down electrons therefore provides a stringent test of this phenomenological ansatz, namely

$$\rho_{yx}^{\text{top}}(B^{\text{eff}}) = \frac{\sigma_{xy}^{\text{OHE},\uparrow}(B^{\text{eff}}) - \sigma_{xy}^{\text{OHE},\downarrow}(B^{\text{eff}})}{(\sigma_{xx}^{\uparrow} + \sigma_{xx}^{\downarrow})^2} \quad (3)$$

so that  $R_{yx}^{\text{top}} = \rho_{yx}^{\text{top}} / B^{\text{eff}}$  is the topological Hall constant. Within the approximation assumed for the relaxation time,  $R_{yx}^{\text{top}}$  does not depend on  $\alpha$  and is thus parameter free.

Shown in Figs. 3(c) and 3(d) are the experimental and calculated dependence of  $R_{yx}^{\text{top}}$  in  $\text{Mn}_{1-x}\text{Fe}_x\text{Si}$  on the ordered magnetic moment. Full symbols correspond to the topological Hall signal at finite temperature, whereas the open symbol corresponds to the estimated zero-temperature value (as explained above this correction is only important in pure MnSi). For pure MnSi the value of about  $3.0 \times 10^{-11} \Omega\text{m/T}$  compares well to the experimental value of  $\sim 4.5 \times 10^{-11} \Omega\text{m/T}$ . Further, upon doping, both the experimental and theoretical variation of  $R_{yx}^{\text{top}}$  exhibit a change of sign and a noticeable reduction in magnitude in reasonable agreement.

According to our calculations all of this can be understood on the basis of the band structure of paramagnetic MnSi in terms of (i) the change of sign of  $\sigma_{xy}^{\text{OHE}}$  for both

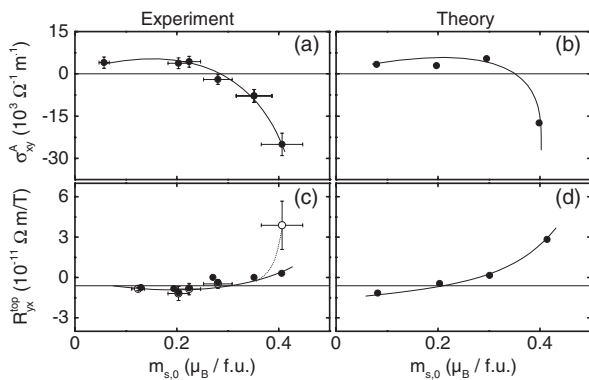


FIG. 3. Anomalous and topological Hall signal as a function of ordered moment in the zero temperature limit. Open symbols denote the extrapolated value for  $T \rightarrow 0$  as described in the Supplemental Material [27]. See text for details.



spin channels, (ii) a significant decrease in magnitude of  $\sigma_{xy}^{\text{OHE},\uparrow}$  as the Fe concentration increases, and (iii) a redistribution of the  $d$  states at the Fermi energy [27]. Graphical illustrations highlighting these observations are shown as part of the Supplemental Material [27]. The change of sign in the OHE is only accessible in our calculations but cannot be determined at low temperatures and small fields.

In summary, the excellent agreement between experiment and microscopic calculations of the AHE and THE in  $\text{Mn}_{1-x}\text{Fe}_x\text{Si}$  reported here provide the long-sought material-specific microscopic justification for the extreme limits of real-space and reciprocal-space Berry phases in a multiband metal with a complex multisheeted Fermi surface. Our study thereby demonstrates the enormous sensitivity of the magnitude of the topological Hall signal to details of the electronic structure, in particular to the Fermi surface topology. Even if the emergent field is very large as in weakly Fe- or Co-doped MnSi, where  $B^{\text{eff}} \approx -15$  T, the THE may vanish altogether.

We wish to thank P. Böni and S. Mayr for helpful discussions and support. C. F., A. B., R. R., C. S., C. D., and T. A. acknowledge financial support through the TUM Graduate School. Financial support through DFG TRR80 and ERC-AdG (291079 TOPFIT) are gratefully acknowledged. F. F. and Y. M. were financially supported under project YIG VH-NG-513 of the Helmholtz Gemeinschaft. F. F., S. B., and Y. M. are grateful to the Jülich Supercomputing Centre for computational time.

- 
- [1] A. Neubauer, C. Pfleiderer, B. Binz, A. Rosch, R. Ritz, P. G. Niklowitz, and P. Böni, *Phys. Rev. Lett.* **102**, 186602 (2009).
- [2] R. Ritz, M. Halder, C. Franz, A. Bauer, M. Wagner, R. Bamler, A. Rosch, and C. Pfleiderer, *Phys. Rev. B* **87**, 134424 (2013).
- [3] R. Ritz, M. Halder, M. Wagner, C. Franz, A. Bauer, and C. Pfleiderer, *Nature (London)* **497**, 231 (2013).
- [4] N. Kanazawa, Y. Onose, T. Arima, D. Okuyama, K. Ohoyama, S. Wakimoto, K. Kakurai, S. Ishiwata, and Y. Tokura, *Phys. Rev. Lett.* **106**, 156603 (2011).
- [5] S. Ishiwata, M. Tokunaga, Y. Kaneko, D. Okuyama, Y. Tokunaga, S. Wakimoto, K. Kakurai, T. Arima, Y. Taguchi, and Y. Tokura, *Phys. Rev. B* **84**, 054427 (2011).
- [6] N. A. Porter, G. L. Creeth, and C. H. Marrows, *Phys. Rev. B* **86**, 064423 (2012).
- [7] P. Sinha, N. A. Porter, and C. H. Marrows, *arXiv*: 1307.7301.
- [8] L. D. Landau and E. M. Lifshitz, *Course of Theoretical Physics* (Pergamon Press, Oxford, UK, 1980), Vol. 8.
- [9] S. Mühlbauer, B. Binz, F. Jonietz, C. Pfleiderer, A. Rosch, A. Neubauer, R. Georgii, and P. Böni, *Science* **323**, 915 (2009).
- [10] W. Münzer, A. Neubauer, T. Adams, S. Mühlbauer, C. Franz, F. Jonietz, R. Georgii, P. Böni, B. Pedersen, M. Schmidt *et al.*, *Phys. Rev. B* **81**, 041203(R) (2010).
- [11] C. Pfleiderer, T. Adams, A. Bauer, W. Biberacher, B. Binz, F. Birkelbach, P. Böni, C. Franz, R. Georgii, M. Janoschek *et al.*, *J. Phys. Condens. Matter* **22**, 164207 (2010).
- [12] X. Z. Yu, Y. Onose, N. Kanazawa, J. H. Park, J. H. Han, Y. Matsui, N. Nagaosa, and Y. Tokura, *Nature (London)* **465**, 901 (2010).
- [13] X. Z. Yu, N. Kanazawa, Y. Onose, K. Kimoto, W. Z. Zhang, Y. Matsui, and Y. Tokura, *Nat. Mater.* **10**, 106 (2011).
- [14] S. Seki, X. Z. Yu, S. Ishiwata, and Y. Tokura, *Science* **336**, 198 (2012).
- [15] T. Adams, A. Chacon, M. Wagner, A. Bauer, G. Brandl, B. Pedersen, H. Berger, P. Lemmens, and C. Pfleiderer, *Phys. Rev. Lett.* **108**, 237204 (2012).
- [16] P. Milde, D. Köhler, J. Seidel, L. M. Eng, A. Bauer, A. Chacon, J. Kindervater, S. Mühlbauer, C. Pfleiderer, S. Buhandt *et al.*, *Science* **340**, 1076 (2013).
- [17] M. Lee, Y. Onose, Y. Tokura, and N. P. Ong, *Phys. Rev. B* **75**, 172403 (2007).
- [18] A. Neubauer, C. Pfleiderer, R. Ritz, P. G. Niklowitz, and P. Böni, *Physica (Amsterdam)* **404B**, 3163 (2009).
- [19] M. Lee, W. Kang, Y. Onose, Y. Tokura, and N. P. Ong, *Phys. Rev. Lett.* **102**, 186601 (2009).
- [20] F. Freimuth, R. Bamler, Y. Mokrousov, and A. Rosch, *Phys. Rev. B* **88**, 214409 (2013).
- [21] F. Freimuth, S. Blügel, and Y. Mokrousov, *J. Phys. Condens. Matter* **26**, 104202 (2014).
- [22] F. Jonietz, S. Mühlbauer, C. Pfleiderer, A. Neubauer, W. Münzer, A. Bauer, T. Adams, R. Georgii, P. Böni, R. A. Duine *et al.*, *Science* **330**, 1648 (2010).
- [23] T. Schulz, R. Ritz, A. Bauer, M. Halder, M. Wagner, C. Franz, C. Pfleiderer, K. Everschor, M. Garst, and A. Rosch, *Nat. Phys.* **8**, 301 (2012).
- [24] A. Bauer, A. Neubauer, C. Franz, W. Münzer, M. Garst, and C. Pfleiderer, *Phys. Rev. B* **82**, 064404 (2010).
- [25] A. Bauer and C. Pfleiderer, *Phys. Rev. B* **85**, 214418 (2012).
- [26] A. Bauer, M. Garst, and C. Pfleiderer, *Phys. Rev. Lett.* **110**, 177207 (2013).
- [27] See Supplemental Material at <http://link.aps.org/supplemental/10.1103/PhysRevLett.112.186601> for the experimental methods and the computational procedures.
- [28] M. Janoschek, M. Garst, A. Bauer, P. Krautscheid, R. Georgii, P. Böni, and C. Pfleiderer, *Phys. Rev. B* **87**, 134407 (2013).
- [29] C. Meingast, Q. Zhang, T. Wolf, F. Hardy, K. Grube, W. Knafo, P. Adelman, P. Schweiss, and H. v. Loehneysen, in *Properties and Applications of Thermoelectric Materials*, edited by V. Zlatic and A. C. Hewson, NATO Science for Peace and Security, Ser. B (Springer, Heidelberg, Germany, 2009), pp. 261–266.
- [30] C. Schnarr, Diploma thesis, Technische Universität München 2012; B. Chapman, M. Grossnickle, T. Wolf, and M. Lee, *Phys. Rev. B* **88**, 214406 (2013).
- [31] T. Adams, Ph. D. thesis, Technische Universität München, 2014.
- [32] T. Adams, J. Kindervater, A. Bauer, S. Mühlbauer, R. Georgii, W. Häußler, B. Böni, and C. Pfleiderer (unpublished).
- [33] In the doped samples we find no evidence for metastable behavior under field cooling as recently observed in pure MnSi at high pressures [2].
- [34] A. A. Mostofi, J. R. Yates, Y.-S. Lee, I. Souza, D. Vanderbilt, and N. Marzari, *Comput. Phys. Commun.* **178**, 685 (2008).
- [35] J. Weischenberg, F. Freimuth, J. Sinova, S. Blügel, and Y. Mokrousov, *Phys. Rev. Lett.* **107**, 106601 (2011).